Proceedings of ASME Turbo Expo 2008: Power for Land, Sea and Air
GT2008
June 9-13, 2008, Berlin, Germany

GT2008-50479

A TIME-DOMAIN FLUID-STRUCTURE INTERACTION ANALYSIS OF FAN BLADES

Seung Ho Cho
Samsung Thales Co., Ltd., Korea

Taehyoun Kim
The Boeing Company, WA

Seung Jin Song
Seoul National University, Korea

ABSTRACT

This paper presents aerodynamic and aeromechanical analyses for an entire row of fan blades (i.e. tens of blades with a finite aspect ratio) subject to a uniform incoming flow. In this regard, a new unsteady three-dimensional vortex lattice model has been developed for multiple blades in discrete time domain. Using the new model, the characteristics of the unsteady aerodynamic forces on vibrating blades, including their temporal development, are examined. Also, the new aerodynamic model is applied to examine the aeromechanical behavior of fan blades by using a standard eigenvalue analysis. For this analysis, the fan blades have been modeled as three-dimensional plates, and, increasing the number of blades (or solidity) is predicted to destabilize the fan blade row.

INTRODUCTION

Fluid-structure interaction phenomena occur in many scientific and engineering applications, including aircraft wings and turbomachinery blades. Understanding fluid structure interactions in turbomachinery is important because such interactions lead to fatigue and ultimately structural damage of blades. The fluid structure interaction analyses require modeling of unsteady aerodynamics which can be conducted in either time or frequency domain. In the time domain analyses, Euler and Navier-Stokes solvers are used to calculate unsteady aerodynamic forces on turbomachinery blades. At each time step, for a given geometry, the flow field is solved to determine the aerodynamic forces acting on the blades. Subsequently, the forces are used to analyze the blades' motions and update their displacements. The entire process is then repeated. Such time domain analyses require extensive computation time and cost [1,2].

On the other hand, unsteady aerodynamic analysis can also be carried out in the frequency domain, and the frequency domain approaches have been applied to calculate unsteady aerodynamic forces acting on two- and three- dimensional cascades [3 - 5]. Such frequency domain analysis can facilitate accurate prediction of flutter onset. However, it is difficult to calculate fatigue and time history under flutter because time does not appear explicitly in the frequency domain analyses.

For multiple blades as in turbomachinery, there are differences in the blades' vibration motions due to aerodynamic and structural couplings. The differences in the blades' motions are manifested as time delays in the time domain or phase differences in the frequency domain. The differences are referred to as the inter-blade phase angle. The number of inter-blade phase angles is identical to the number of blades. In the frequency domain, many researchers have investigated flutter by prescribing the inter-blade phase angle for cascades with an infinite number of blades [4, 6-9] or for a few passages [1, 10, and 11].

More recently, more ambitious numerical approaches focusing on entire blade rows or even multiple stages have been reported in the literature. He et al. [12] coupled frequency domain aerodynamics with a reduced order model of the bladed disc assembly to study mistuning effects in an industrial fan. Gottfried and Fleeter [13] used a finite element method in time domain to examine aerodynamic damping in a modern transonic compressor blade row. Sadeghi and Lui investigated turbine cascade flutter with an unsteady Euler solver [14], and Carstens et al. used a Navier-Stokes solver to examine a transonic rotor [15]. Sayma et al. and Vahdati et al. have even reported computing all seventeen stages of a compressor [16,17]. Alternatively, Johnston et al. [18] have attempted to couple commercially available computational fluid dynamic (CFD) and computational structural dynamic (CSD) programs to solve turbomachinery aeroelasticity problems. However, such approaches are computationally expensive and are not yet amenable for routine design use.

On the other hand, Hall [19] has proposed an eigen formulation for unsteady aerodynamic forces for airfoils, cascades, and wings in the discrete time domain. Kim et al. [20] extended the method to continuous time domain. Cho et al. [21] have developed a vortex lattice model in discrete time domain to analyze the aeroelastic stability of an isolated two-dimensional airfoil under pulsating freestream conditions. These methods can also predict aeroelastic stability, and are computationally less costly than unsteady CFD approaches. So far, however, such analyses have been limited to an isolated airfoil or a two-dimensional cascade with an infinite number of blades. Therefore, approximate but fast analytical methods to predict aerodynamic and aeromechanical behaviors of an entire blade row (with tens of blades) are needed.

This paper presents a new time domain aerodynamic model for analyzing unsteady aerodynamic forces on a three dimensional turbomachinery blade row under a uniform incoming flow. A new unsteady aerodynamic model, based on the vortex lattice method, is first presented and the model's predictions are discussed. Subsequently, the new aerodynamic model is applied to a structural model of a fan assembly (i.e. flexible blades connected to a rigid disc) to predict the fan assembly's aeromechanical behavior.

NOMENCLATURE

A	=	extension stiffness matrix; plate area
AR	=	aspect ratio
B	=	extension/bending coupling stiffness matrix; total number of blades
BML	=	total number of vortex ring elements on all blades
BNL	=	total number of bound and wake vortex elements on all blades
c	=	blade chord
D	=	bending stiffness matrix
$e_\perp$	=	direction out of blade plane
J	=	kernel function
K	=	stiffness matrix
k	=	index number of blade
L	=	total number of spanwise direction elements; generalized aerodynamic force
l	=	blade span
M	=	mass matrix; in-plane moment
$M1$	=	total number of vortex ring elements in blade
N	=	in-plane force
$N1$	=	total number of vortex elements in blade
n	=	time level; total number of mode shapes
q	=	state vector; velocity induced by vortex segment
R_H	=	hub radius
s	=	blade pitch
T	=	kinetic energy
U	=	freestream velocity; strain energy
u	=	chordwise displacement
v	=	spanwise displacement
W	=	work
w	=	downwash velocity; out-of-plane displacement
z	=	state vector
α	=	weighting factor
Γ	=	vortex strength
γ	=	mode shape
Δt	=	size of time steps
Δx	=	size of chordwise direction elements
Δr	=	size of spanwise direction elements
ε	=	midplane strain
θ	=	angle between each plane of blade
κ	=	midplane curvature
ρ	=	structure density
ρ_∞	=	fluid density
σ	=	inter-blade phase angle
ϕ	=	chordwise mode shape
χ	=	spanwise mode shape

Subscript

a	=	aerodynamic
s	=	structure
1	=	on blade; chordwise bending
2	=	in wake; spanwise bending
3	=	torsional

MODEL DESCRIPTION

A. Unsteady Aerodynamic Model

A three-dimensional unsteady vortex lattice method for multiple blades has been developed to calculate unsteady aerodynamic forces on turbomachinery blades (Fig. 1). The new three-dimensional unsteady aerodynamic model assumes an inviscid, incompressible, and irrotational flow coming into a turbomachinery blade row. In the current study, multiple blades and their aerodynamic interactions are considered, but effects such as engine casing and deviation are not accounted for. The number of blades is B. The first blade is in the chordwise (x) – spanwise (r) direction plane, and the plane of the next blade is rotated at angle $\theta = 2\pi/B$ in the circumferential direction. On each blade, the bound and free vortices representing the blade and traveling wake, respectively, are composed of a finite number of vortex ring elements. There are M elements in the chordwise direction, and L elements in the spanwise direction on each blade. There are (N-M) elements in the chordwise direction in the wake of each blade. Thus, the total number of vortex ring elements is BML(=B x M x L) for all blades and BNL(=B x N x L) for all blades and wakes. The elements are all of equal size Δx by Δr on each blade. The element at the i, j-th location in the x and r coordinates at the k-th blade is assigned a vortex strength Γ_{ijk}.

For convenience, a (L x 1) vector ${}^{k}_{i}\Gamma$ is defined as

$$ {}^{k}_{i}\Gamma = \begin{bmatrix} \Gamma_{i1k} & \Gamma_{i2k} & \cdots & \Gamma_{iLk} \end{bmatrix}^T \quad (L \text{ x } 1) \qquad (1) $$

With this definition, the downwash vector can be expressed in the discrete time domain as

$$ w^n = \begin{bmatrix} w_1^n & w_2^n & \cdots & w_B^n \end{bmatrix}^T = \begin{bmatrix} J_1^n & J_2^n \end{bmatrix} \begin{Bmatrix} \Gamma_1^n \\ \Gamma_2^n \end{Bmatrix} \qquad (2) $$

where its i-th component w_i^n is a (ML x 1) vector containing the downwashes at three-quarter points of the vortex elements of the i-th blade at the n-th time step. A bound vortex vector Γ_1 (BML x 1) is defined as

$$ \Gamma_1 = \begin{bmatrix} {}^{1}\Gamma_1 & {}^{2}\Gamma_1 & \cdots & {}^{B}\Gamma_1 \end{bmatrix}^T \quad (BML \text{ x } 1) \qquad (3) $$

where

$$ {}^{k}\Gamma_1 = \begin{bmatrix} {}^{k}_{1}\Gamma & {}^{k}_{2}\Gamma & \cdots & {}^{k}_{M}\Gamma \end{bmatrix}^T \quad (ML \text{ x } 1) \qquad (4) $$

Similarly, a wake vortex vector Γ_2 ((BNL-BML) x 1) is defined as

$$ \Gamma_2 = \begin{bmatrix} {}^{1}\Gamma_2 & {}^{2}\Gamma_2 & \cdots & {}^{B}\Gamma_2 \end{bmatrix}^T \quad ((BNL\text{-}BML) \text{ x } 1) \qquad (5) $$

where

$$ {}^{k}\Gamma_2 = \begin{bmatrix} {}^{k}_{M+1}\Gamma & {}^{k}_{M+2}\Gamma & \cdots & {}^{k}_{N}\Gamma \end{bmatrix}^T \quad ((NL\text{-}ML) \text{ x } 1) \qquad (6) $$

Γ_1 and Γ_2 represent arrays of vortex strengths for the blades and wakes, respectively. For a vortex ring element in a three-dimensional incompressible flow, the kernel function J_{ij} of a unit vortex strength at the j-th vortex point influences the velocity at the i-th collocation point. The collocation points are located at the three-quarter chord point in the streamwise direction and the central point in the spanwise direction of bound vortex elements. The vortex points are located at the quarter chord point in the streamwise direction and the central point in the spanwise direction of bound and free vortex elements [22]. Given a vortex strength Γ, the velocity induced by a vortex segment lm is

$$ q_{lm}(x,y,z) = \frac{\Gamma}{4\pi} \frac{\vec{r}_l \times \vec{r}_m}{\left|\vec{r}_l \times \vec{r}_m\right|^2} \left[\vec{r}_0 \cdot \left(\frac{\vec{r}_l}{r_l} - \frac{\vec{r}_m}{r_m} \right) \right] \qquad (l, m = 1, 2, 3, 4) \qquad (7) $$

The total velocity induced by a vortex ring element is the sum of q_{lm} for all four segments as follows.

$$ q^{tot} = q_{12} + q_{23} + q_{34} + q_{41} = q_i^{tot}\hat{i} + q_j^{tot}\hat{j} + q_k^{tot}\hat{k} \qquad (8) $$

The kernel function J_{ij} is the vertical component of each blade's plane with respect to q^{tot} per unit vortex strength and is located at the c/4 of the vortex ring element as follows.

$$ J_{ij} = \frac{\hat{e}_\perp \cdot q^{tot}}{\Gamma} \qquad (9) $$

where $\hat{e}_\perp$ is a unit vector out of each blade's plane.

The conservation of vorticity in the k-th blade is

$$ {}^{k}_{M+1}\Gamma^{n+1} = {}^{k}_{M}\Gamma^{n} \qquad (k = 1, 2, \ldots, B) \qquad (10) $$

The convection of free wakes in the k-th blade is described in the discrete time domain as follows.

$$ {}^{k}_{i}\Gamma^{n+1} = {}^{k}_{i-1}\Gamma^{n} \quad (i = M+2, \ldots, N\text{-}1,\ k = 1,2,\ldots,B) \qquad (11) $$

$$ {}^{k}_{N}\Gamma^{n+1} = \alpha\left({}^{k}_{N}\Gamma^{n}\right) + {}^{k}_{N-1}\Gamma^{n} \quad (k = 1,2,\ldots,B,\ 0.95<\alpha<1) \qquad (12) $$

With the weighting factor α in Eq. (12), one can cut off the infinitely long wake vortex at a finite length. For a uniform inflow, Hall [12] suggests $0.95<\alpha<1$.

Combining the equation for downwash [Eq. (2)], conservation of vorticity [Eq. (10)], and free wake convection [Eqs. (11) and (12)] leads to

$$ \Gamma_2^{n+1} = A\Gamma_1^n + B\Gamma_2^n \qquad (13) $$

To reduce the size of the equation, the bound vortex Γ_1^n is eliminated by using static condensation as follows (Kim et al. [13]). Solving for Γ_1^n from the kernel function, Eq. (2) gives

$$ \Gamma_1^n = -J_1^{-1}J_2^n\Gamma_2^n + J_1^{-1}w^n \qquad (14) $$

Equation (14) is then substituted into Eq. (13) to give

$$ \Gamma_2^{n+1} = \left\{B - A\left(J_1^n\right)^{-1}J_2^n\right\}\Gamma_2^n + A\left(J_1^n\right)^{-1}w^n = A_a\Gamma_2^n + B_a w^n \qquad (15) $$

B. Structural Model

The blades are modeled as three-dimensional plates. Blades' thickness and camber effects are not accounted for in the structural model. The disc to which blades are attached is assumed to be rigid. Forces and moments acting on a three-dimensional plate are derived for the classical three-dimensional plate. The equation of motion of the k-th blade is

$$ {}^{k}M\left({}^{k}\ddot{q}\right) + {}^{k}K\left({}^{k}q\right) = {}^{k}L \qquad (16) $$

Using the displacement expressions, the strain energy and kinetic energy are written in matrix form as

$$ U = \frac{1}{2}q^T Kq \qquad (17) $$

$$ T = \frac{1}{2}\dot{q}^T M\dot{q} \qquad (18) $$

where K and M are the generalized stiffness and mass matrices, respectively. They are defined as

$$ {}^{k}M_{ij} = \iint_A {}^{k}\rho \gamma_i \gamma_j \, dxdr \tag{19} $$

$$ {}^{k}K_{ij} = \iint_A \left[\begin{array}{l} {}^{k}D_{11} \dfrac{\partial^2 \gamma_i}{\partial x^2} \dfrac{\partial^2 \gamma_j}{\partial x^2} + {}^{k}D_{22} \dfrac{\partial^2 \gamma_i}{\partial r^2} \dfrac{\partial^2 \gamma_j}{\partial r^2} \\ + 4\left({}^{k}D_{33}\right) \dfrac{\partial^2 \gamma_i}{\partial x \partial r} \dfrac{\partial^2 \gamma_j}{\partial x \partial r} \\ + {}^{k}D_{12} \left\{ \dfrac{\partial^2 \gamma_i}{\partial x^2} \dfrac{\partial^2 \gamma_j}{\partial r^2} + \dfrac{\partial^2 \gamma_i}{\partial r^2} \dfrac{\partial^2 \gamma_j}{\partial x^2} \right\} \\ + 2\left({}^{k}D_{13}\right) \left\{ \dfrac{\partial^2 \gamma_i}{\partial x^2} \dfrac{\partial^2 \gamma_j}{\partial x \partial r} + \dfrac{\partial^2 \gamma_i}{\partial x \partial r} \dfrac{\partial^2 \gamma_j}{\partial x^2} \right\} \\ + 2\left({}^{k}D_{23}\right) \left\{ \dfrac{\partial^2 \gamma_i}{\partial r^2} \dfrac{\partial^2 \gamma_j}{\partial x \partial r} + \dfrac{\partial^2 \gamma_i}{\partial x \partial r} \dfrac{\partial^2 \gamma_j}{\partial r^2} \right\} \end{array} \right] dxdr \tag{20} $$

where ${}^{k}D_{11}$, ${}^{k}D_{22}$, ${}^{k}D_{33}$, ${}^{k}D_{12}$, ${}^{k}D_{13}$, and ${}^{k}D_{23}$ represent chordwise bending, spanwise bending, torsional, chordwise bending-spanwise bending coupling, chordwise bending-torsion coupling, and spanwise bending-torsion coupling of the *k*-th blade, respectively.

The structural model of the *k*-th blade is given in time as follows.

$$ \left\{ \begin{matrix} {}^{k}\dot{q} \\ {}^{k}\ddot{q} \end{matrix} \right\} = \left[\begin{matrix} O & I \\ -{}^{k}M^{-1}\left({}^{k}K\right) & O \end{matrix} \right] \left\{ \begin{matrix} {}^{k}q \\ {}^{k}\dot{q} \end{matrix} \right\} + \left[\begin{matrix} O \\ {}^{k}M^{-1} \end{matrix} \right] {}^{k}L \tag{23} $$

Discretizing Eq. (23) in time, a discrete time domain form for the *k*-th blade is obtained as follows.

$$ {}^{k}z^{n+1} = {}^{k}A_s\left({}^{k}z^{n}\right) + {}^{k}B_s\left({}^{k}L^{n}\right) \tag{24} $$

where ${}^{k}z$ is a state vector, $[{}^{k}q \;\; {}^{k}\dot{q}\,]^T$.

For convenience, a ((*B* x 2*n*)x 1) vector *z* is defined as

$$ z = \left[{}^{1}z \quad {}^{2}z \quad \cdots \quad {}^{B}z \right]^T \qquad ((B \text{ x } 2n) \text{x } 1) \tag{25} $$

Equation (24) is then extended to *B* blades to yield

$$ z^{n+1} = A_s z^{n} + B_s L^{n} \tag{26} $$

The generalized aerodynamic force component for the *i*-th mode shape of the *k*-th blade can be approximated as

$$ {}^{k}L_i = \iint_A \Delta^{k}p(x,r,t)\gamma_i(x,r)\,dxdr \cong \sum_{l=1}^{L}\sum_{m=1}^{M} \Delta^{k}p_{ml}\phi_i(x_m)\psi_i(r_l)\Delta x \Delta r $$
$$ (i = 1, 2, \ldots, n,\ k = 1, 2, \ldots, B) \tag{27} $$

where the subscripts *m* and *l* stand for the location of the (*m*, *l*)-th vortex of strength Γ_{ml}. Using the unsteady Bernoulli equation, the pressure differential on the *k*-th blade can be expressed as [15].

$$ \Delta^{k}p_{ml} = \Delta^{k}p(x_m, y_l, t) = \rho_\infty \left\{ {}^{k}U(t)\left(\frac{\Gamma_{mlk} - \Gamma_{m-1lk}}{\Delta x} \right) + \dot{\Gamma}_{mlk} \right\} \tag{28} $$

where the freestream velocity ${}^{k}U(t)$ is time-varying. Using a forward difference formula, $\dot{\Gamma}_{mlk}$ can be written in discrete-time domain as follows.

$$ \dot{\Gamma}_{mlk} \cong \frac{\Gamma_{mlk}^{n+1} - \Gamma_{mlk}^{n}}{\Delta t} \tag{29} $$

Equations (28) and (29) are then substituted into Eq. (27) to give

$$ {}^{k}L_i^{n} = {}^{k}U(n\Delta t)V_1\left({}^{k}\Gamma_i^{n}\right) + U_\infty V_2\left({}^{k}\Gamma_i^{n+1} - {}^{k}\Gamma_i^{n}\right) \tag{30} $$

For blades undergoing out-of-plane motion *w*(*x*, *y*, *t*), the downwash vector in the *k*-th blade is related to the generalized coordinates as

$$ {}^{k}w = {}^{k}U(t)E_1\left({}^{k}q\right) + E_2\left({}^{k}\dot{q}\right) \tag{31} $$

where the elements of the E_1, E_2 matrices are given as

$$ e_{1ij} = \frac{\partial \phi_j(x_{pi})}{\partial x}\psi_j(r_{pi}) $$
$$ (i = 1, 2, \ldots, M1,\ j = 1, 2, \ldots, n) \tag{32} $$

$$ e_{2ij} = \phi_j(x_{pi})\psi_j(y_{pi}) $$
$$ (i = 1, 2, \ldots, M1,\ j = 1, 2, \ldots, n) \tag{33} $$

Here, the subscript *pi* stands for the location of the *i*-th collocation point.

C. Aeroelastic Model

Combining the unsteady aerodynamic equation [Eq. (15)], the structural equation [Eq. (26)], the generalized aerodynamic force equation [Eq. (30)], and the downwash vector equation [Eq. (31)] leads to the aeroelastic system of equations. The resulting system of (*B* x (*NL*-*ML*+2*n*)) equations with no gust velocity is as follows.

$$ \left[\begin{matrix} I & O \\ O & I - B_s B_{3,4} \end{matrix} \right] \left\{ \begin{matrix} \Gamma_2 \\ z \end{matrix} \right\}^{n+1} = \left[\begin{matrix} A_a & B_a E_{1,2} \\ B_s A_1 & A_s + B_s B_{1,2} \end{matrix} \right] \left\{ \begin{matrix} \Gamma_2 \\ z \end{matrix} \right\}^{n} \tag{34} $$

MODEL PREDICTIONS

A. Unsteady Aerodynamic Results

A row of fan blades with an aspect ratio of 3.3 has been chosen for the current analysis. The input parameters of the fan blades are based on Kaza and Kielb [8]. Table 1 lists the relevant geometries of the fan blades. The blades have a pitch to chord ratio *s*/*c* of 0.46 at the hub and 1.21 at the tip. Twenty eight blades are considered in the current study, and, hence, there are 28 inter-blade phase angle modes under a uniform inflow. The new model's predictions for a single blade have been examined in a separate paper by Cho et al. [23]. For an isolated blade, as the aspect ratio increases, the model's predicted nondimensional lift approaches the analytical two-dimensional solution (Fig. 2 [23]).

Figure 3 shows the computed indicial response of the 28 blades for inter-blade phase angles of 0° and 180°. To calculate the indicial response, a step change in the downwash of blades is required. The step change in the downwash of blades can be imposed in the same or opposite directions between adjacent blades. The downwashes with the same and opposite directions between adjacent blades correspond to the motion with the inter-blade phase angles (σ) of 0° and 180°, respectively. For σ = 180°, the indicial lifts of adjacent blades have the same magnitude but opposite signs because the opposite vortices induced by the downwash vectors between the adjacent blades lead to opposite unsteady lifts between the adjacent blades (via the unsteady Bernoulli equation [Eq. (28)]). On the other hand, for σ = 0°, the indicial lift on all blades have the same value because the downwash vectors and vortices on all blades are identical.

The downwash on the reference blade is induced by the vortices on the adjacent blades (called the adjacent blade vortices) as well as the vortices on the reference blade (called the reference blade vortices) via the kernel function [Eq. (2)]. However, the unsteady lift on the reference blade is induced only by the reference blade vortices. In Fig. 3, the indicial response for σ = 180° is larger than that in a single blade and σ = 0°. For σ = 180°, the adjacent blade vortices and the reference blade vortices have opposite signs. Therefore, to induce a step change in the downwash, stronger reference blade vortices are required for multiple blades with σ = 180° than for a single blade. As only the reference blade vortices induce unsteady lift, the unsteady lift is increased. On the other hand, to induce a step change in the downwash, weaker reference blade vortices are required for multiple blades with σ = 0° than for a single blade. Therefore, the unsteady lift is reduced for σ = 0°. Thus, the unsteady aerodynamic forces depend on the inter-blade phase angle.

Figure 4 shows the computed indicial lift under a uniform inflow due to a step change for various blade numbers when the inter-blade phase angle is 180°. In the figure, increasing the blade number (or decreasing the pitch to chord ratio *s*/*c* in Fig. 1) increases the unsteady lift. This result is due to the strengthening of the adjacent blade vortices because the influence of vortices is proportional to the inverse of the distance between adjacent blades (Eq. 7). With increasing number of blades, to induce a downwash of a magnitude equal to that with fewer blades, the reference blade vortices are strengthened in response to the strengthening of adjacent blade vortices with opposite signs. Thus, the unsteady lift increases. Figure 5 shows the corresponding indicial lift when the inter-blade phase angle is 0°. Contrary to σ = 180°, increasing the blade number decreases the unsteady lift because the adjacent blade vortices and the reference blade vortices have the same sign. With many blades, the reference blade vortices may have a smaller absolute value because of the adjacent blade vortices with same sign, and thus the unsteady lift decreases.

B. Aeroelastic Stability Results

A plate model with the first four modes – the first bending mode q_1, the first torsion mode q_2, the second bending mode q_3, and the second torsion mode q_4 – has been adopted as the structural model for each blade. For 28 vibrating blades, the total number of structural modes is 28 x 4 = 112. Listed in Table 2 are the values of material properties of the fan blades used in the current study. The values of material properties are based on Dunn and Dugundji [24].

The stability of an aeroelastic system changes with the blade number. Figure 6 shows the flutter speed under a uniform inflow plotted versus the blade number. The flutter speed decreases linearly with the total blade number because increasing the blade number decreases the blade pitch to chord ratio (*s*/*c*). Decreasing the blade pitch to chord ratio pushes the blades closer to each other, and strengthens the kernel function via the Biot-Savart rule. Thus, increasing the blade number destabilizes aeroelastic systems.

The inter-blade phase angle (IBPA) can also be predicted by the new time-domain model. For this proof-of-concept calculation, the blade number has been assumed to be 12 instead of 28 to reduce computation time (Calculation of 28 blades is more time consuming but possible). Figures 7 (a) to (g) show the eigenmodes of blades near the flutter speed. In the figure, the real value of the first torsional eigenmodes is plotted versus the blade index. In Fig. 7 (a), Mode 0 means an inter-blade phase angle of 0° because the real values of the first torsional eigenmodes of all blades are identical and there is no peak. Mode 1 in Fig. 7 (b) has one peak per one period, indicating an inter-blade phase angle of 30°. Similarly, Modes 2 to 6 mean σ = 60°, … , 180°, respectively. Modes for σ = 210°, … , 330° are similar to those for σ = 150°, … , 30°, respectively. Thus, there are two single modes (Modes 0 and 6) and five pairs of modes (Modes 1 to 5), and the total number of modes or inter-blade phase angles is 12, which is identical to the blade number.

Dugundji and Bundas [6] report flutter velocity occurring at σ = 40° for their nine-bladed rotor. In the current 12-bladed fan case, however, the mode for σ = 180° flutters first. The difference between the current study and Dugundji & Bundas

can be attributed as follows. First, Dugundji and Bundas [6] use Whitehead's [7 and 9] frequency domain analysis for a two-dimensional cascade with an infinite number of blades. In Whitehead's approach, only one inter-blade phase angle is imposed as an input parameter, and then the flutter speed for that particular inter-blade phase angle is calculated. Also, by assuming a single inter-blade phase angle at a time, they are implicitly coupling the blades structurally. However, in the current study, such inter-blade phase angles are not assumed a priori. Thus, in this study, the blades are coupled to each other only aerodynamically. Under such circumstances, the modes near $\sigma = 180^\circ$ first become unstable because the largest amount of aerodynamic work is imparted onto the blades at inter-blade phase angle near 180°.

CONCLUSIONS

The new conclusions of this paper can be summarized as follows:

1. A new three-dimensional unsteady vortex lattice model has been developed to analyze unsteady aerodynamics and aeroelastic stability of an entire turbomachinery blade row.

2. Unsteady aerodynamic forces depend on the inter-blade phase angles, and the indicial lift for an inter-blade phase angle of 180° is larger than that for 0°.

3. Increasing the blade number increases the unsteady lift for an inter-blade phase angle of 180°, but the relationship is reversed for an inter-blade phase angle of 0°.

4. For fan blades which are modeled to be aerodynamically coupled but structurally independent, the first torsional mode nearest $\sigma = 180^\circ$ first becomes unstable.

5. For a blade row, increasing the number of blades decreases the flutter speed and destabilizes the aeroelastic system.

APPENDIX

The in-plane forces and moments of each three-dimensional blade are obtained by integrating stresses over thickness and are expressed as follows [25-27].

$$N = \int \sigma de_{\perp} = A\varepsilon + B\kappa \tag{A.1}$$

$$M = \int \sigma z de_{\perp} = A\varepsilon + B\kappa \tag{A.2}$$

where ε and κ are the midplane strain and curvature, respectively. Furthermore, A, D, and B are the extension, bending, and extension/bending coupling stiffness matrices, respectively.

Using the Rayleigh-Ritz formulation, strain energy, kinetic energy, and work of each blade can be expressed as

$$U = \frac{1}{2}\iint_A \begin{bmatrix} \varepsilon & \kappa \end{bmatrix} \begin{bmatrix} A & B \\ B & D \end{bmatrix} \begin{Bmatrix} \varepsilon \\ \kappa \end{Bmatrix} dxdr \tag{A.3}$$

$$T = \frac{1}{2}\iint_A \rho \left\{ \left(\frac{\partial u}{\partial t}\right)^2 + \left(\frac{\partial r_{disp}}{\partial t}\right)^2 + \left(\frac{\partial e_{\perp disp}}{\partial t}\right)^2 \right\} dxdr \tag{A.4}$$

$$W = \iint_A \Delta p(x,r,t) e_{\perp disp}(x,r,t) dxdr \tag{A.5}$$

where A represents blade area. u, r_{disp}, and $e_{\perp disp}$ are the displacements in the x, r, and $e_{\perp}$ directions, respectively.

To represent the out-of-plane displacement $e_{\perp disp}(x, y, t)$ of each blade, a set of mode shapes has been used.

$$u(x,r,t) = 0 \tag{A.6}$$

$$r_{disp}(x,r,t) = 0 \tag{A.7}$$

$$e_{\perp disp}(x,r,t) = \sum_{i=1}^{n} \gamma_i(x,r) q_i(t) \tag{A.8}$$

The i-th mode shape $\gamma_i(x, r)$ is assumed to be a product of separate mode shapes in x and r directions as

$$\gamma_i(x,r) = \phi_i(x)\psi_i(r) \tag{A.9}$$

Free-free beam vibration modes in the x direction are [21]

$$\phi_i(x) = \begin{cases} 1 & (i = \text{odd number}) \\ -2\sqrt{3}\dfrac{x}{c} & (i = \text{even number}) \end{cases} \tag{A.10}$$

where harmonic modes are ignored. On the other hand, cantilever beam vibration modes for the rotor blades are used in the spanwise (r) direction as follows.

$$\psi_i(r) = \left(-\cos\bar{\alpha}_i \frac{R_H + r}{l} + \cosh\bar{\alpha}_i \frac{R_H + r}{l} \right) + \bar{\beta}_i \left(-\sin\bar{\alpha}_i \frac{R_H + r}{l} + \sinh\bar{\alpha}_i \frac{R_H + r}{l} \right) \quad (i = 1, 2, 3, \ldots) \tag{A.11}$$

where R_H is hub radius. $\psi_i(r)$ has to be chosen properly to satisfy the boundary conditions. The mode shapes become bending and torsional when i becomes odd and even, respectively. For a blade clamped at the root, w and $\partial w/\partial y$ are zero at the root.

The Lagrange's equation is

$$\frac{d}{dt}\left(\frac{\partial T}{\partial \dot{q}_i}\right) - \frac{\partial T}{\partial q_i} + \frac{\partial U}{\partial q_i} = L_i \quad (i = 1, 2, \ldots, n) \tag{A.12}$$

Substituting the strain energy [Eq. (A.3)], kinetic energy [Eq. (A.4)], and work [Eq. (A.5)] of each blade to the

Lagrange's equation [Eq. (A.12)] leads to the equation of motion of the *k*-th blade as follows.

$$ {}^{k}M\left({}^{k}\ddot{q}\right)+{}^{k}K\left({}^{k}q\right)={}^{k}L \qquad \text{(A.13)} $$

ACKNOWLEDGMENTS

The authors are grateful to Professor Sang Joon Shin of Seoul National University for his helpful comments. Also, the authors acknowledge the second stage of the BK 21 Project, the Microthermal System Research Center of the Korea Science and Engineering Foundation, and the Institute of Advanced Machinery and Design of Seoul National University.

REFERENCES

[1]Doi, H., "Fluid/Structure Coupled Aeroelastic Computations for Transonic Flows in Turbomachinery," Ph.D. Thesis, Stanford University, Palo Alto, CA, 2002.

[2]Kazawa, J. and Watanabe, T., "Numerical Analysis toward Active Control of Cascade Flutter with Smart Structure," *The 38th AIAA/ASME/SAE/ASEE Joint Propulsion Conference and Exhibit*, AIAA 2002-4079, AIAA, Washington, DC, 2002.

[3]Whitehead, D. S. and Grant, R. J., "Force and Moment Coefficients of High Deflection Cascades," *Proceedings of the 2nd International Symposium on Aeroelasticity in Turbomachines*, edited by P. Suter, Juris-Verlag, Zurich, Switzerland, 1981, pp. 85-127.

[4]Verdon, J. M. and Casper, J. R., "A Linearized Unsteady Aerodynamic Analysis for Transonic Cascades," *Journal of Fluid Mechanics*, Vol. 149, Dec. 1984, pp. 403-429.

[5]Holmes, D. G. and Chuang, H. A., "2D Linearized Harmonic Euler Flow Analysis for Flutter and Forced Response," *Unsteady Aerodynamics, Aeroacoustics, and Aeroelasticity of Turbomachines and Propellers*, edited by H. M. Atassi, Springer-Verlag, New York, 1993, pp. 213-230.

[6]Dugundji, J., and Bundas, D. J., "Flutter and Forced Response of Mistuned Roters Using Standing Wave Analysis," *AIAA Journal*, Vol. 22, No. 11, 1984, pp. 1652-1661. Also available as NASA CR-173555.

[7]Whitehead, D. S., "Force and Moment Coefficients for Vibrating Airfoils in Cascade," British Aeronautical Research Council, Reports and Memoranda No. 3254, London, 1960.

[8]Kaza, K. R. V. and Kielb, R. E., "Flutter of Turbofan Rotors with Mistuned Blades," *AIAA Journal*, Vol. 22, No. 11, Nov. 1984, pp. 1618-1625.

[9]Whitehead, D. S., "Classical Two-Dimensional Methods," *AGARD Manual on Aeroelasticity in Axial Flow Turbomachines. Vol. 1: Unsteady Turbomachinery Aerodynamics*, edited by M. F. Platzer, and F. O. Carta, AGARD, Neuilly-sur-Seine, France, AGARD-AG-298, Vol. 1, March 1987, Chap. 3.

[10]Florea, R., "Reduced Order Modeling and Eigenvalue Analysis of Unsteady Flows about Oscillating Airfoils and Turbomachinery Cascades," Ph.D. Thesis, Duke University, Durham, NC, 1996.

[11]Epureanu, B. I., "Reduced Order, Inviscid and Fully Simultaneous Viscous-Inviscid Interaction Models of Flows in Turbomachinery," Ph.D. Thesis, Duke University, Durham, NC, 1999.

[12]He, Z., Epureanu, B., and Pierre, C., "Fluid-Structural Coupling Effects on the Dynamics of Mistuned Discs", AIAA Journal, Vol. 45, No. 3, pp. 552-561, 2007.

[13]Gottfried, D. and Fleeter, S., "Aeroydnamic Damping Predictions in Turbomachines Using a Coupled Fluid-Structure Model", Journal of Propulsion and Power, Vol. 21, No. 2, pp. 327-335, 2005.

[14]Sadeghi, M. and Liu, F., "Investigation of Mistuning Effects on Cascade Flutter Using a Coupled Method", Journal of Propulsion and Power, Vol. 23, No. 2, pp. 266-, 2007.

[15]Carstens, V., Kemme, R., and Schmitt, S., "Coupled Simulation of Flow-Structure Interaction in Turbomachinery", aerospace Science and Technology, Vol. 7, pp. 298-306, 2003.

[16]Sayma, A. I., Vahdati, M., and Imregun, M., "An Integrated Nonlinear Approach for Turbomachinery Forced Response Prediction. Part I: Formulation", Journal of Fluids and Structures, Vol. 14, pp. 87-101, 2000.

[17]Vahdati, M., Sayma, A., and Imregun, M., "An Integrated Nonlinear Approach for Turbomachinery Forced Response Prediction. Part II: Case Studies", Journal of Fluids and Structures, Vol. 14, pp. 103-125, 2000.

[18]Johnston, D., Cross, C., and Wolff, J., "An Architecture for Fluid/Structure Inateraction Analysis of Turbomachinery Blading", AIAA 2005-4013, 41st AIAA/ASME/SAE/ASEE Joint Propulsion Conference & Exhibit, Tucson, Arizona, July, 2005.

[19]Hall, K. C., "Eigenanalysis of Unsteady Flows about Airfoils, Cascades, and Wings," *AIAA Journal*, Vol. 32, No. 12, 1994, pp. 2426-2432.

[20]Kim, T. H., Nam, C. H., and Kim, Y. D., "Reduced-order Aeroservoelastic Model with an Unsteady Aerodynamic Eigenformulation," *AIAA Journal*, Vol. 35, No.6, 1997, pp. 1087, 1088.

[21]Cho, S. H., Kim, T., Song, S. J., and Shin, S. J., "Aeroelastic Analysis of an Isolated Airfoil Under a Pulsating Flow," *AIAA Journal*, Vol. 45, No. 5, 2007, pp. 1000-1006.

[22]Katz, J. and Plotkin, A., *Low-Speed Aerodynamics*, 2nd ed., Cambridge University Press, UK, 2001.

[23]Cho, S. H., Kim, T., and Song, S. J., "Aeromechanical Analysis of an Isolated Three-Dimensional Blade under a Pulsating Freestream," *AIAA Journal* (Submitted).

[24]Dunn, P. E. and Dugundji, J, "Nonlinear Stall Flutter and Divergence Analysis of Cantilevered Graphite/Epoxy Wings," *AIAA Journal*, Vol. 30, No. 1, 1992, pp. 153-162.

[25]Jones, R. M., *Mechanical of Composite Materials*, 2nd ed., McGraw-Hill Book Co., USA, 1975.

[26]Whitney, J. M., *Structural Analysis of Laminated Anisotropic Plates*, Technomic Publishing Co. Inc., USA, 1987.

[27]Cook, R. D., Malkus, D. S., and Plesha, M. E., *Concepts and Applications of Finite Element Analysis*, 3rd ed., John Wiley & Sons, USA, 1989.

ANNEX A

Table 1. Reference quantities of a fan blade [8]

Parameters	Values
Aspect ratio	3.3
Number of blades	28
Chord length	0.1892 m
Hub radius	0.3876 m
Span length	0.6334 m
Air density	1.0 kg/m^2

Table 2. Structural parameters of the multiple blade model [17]

Parameters	Values
Chord length	0.1892 m
Span length	0.6334 m
Aspect ratio	3.3
Material density for plate	3.046 kg/m^2
Thickness of plate	0.002 m
Spanwise bending stiffness	433.3 kgm^2/s^2
Torsional stiffness	37.56 kgm^2/s^2

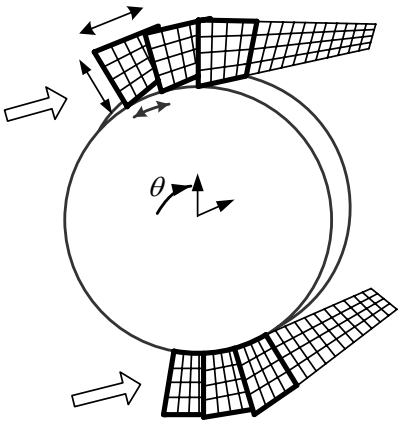

Figure 1. Domain for unsteady lifting-surface solution of multiple blades.

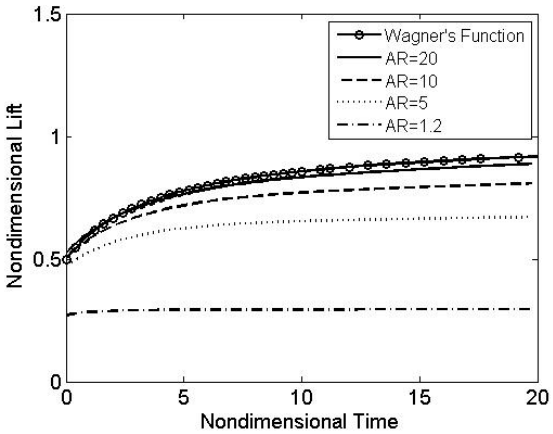

Figure 2. Indicial lift of a single blade for various aspect ratios [16].

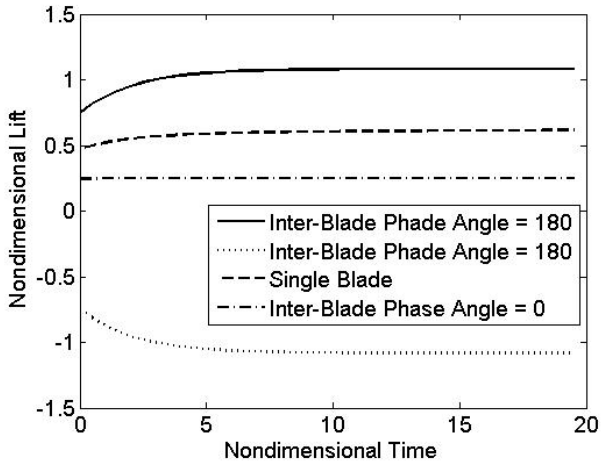

Figure 3. Indicial lift under a uniform flow due to a step input for two different inter-blade phase angle of 28 blades.

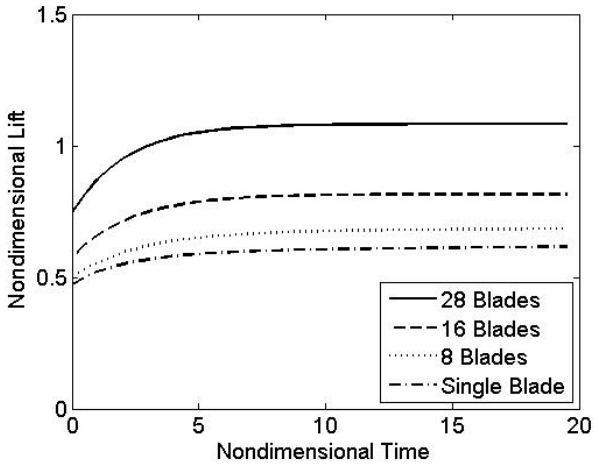

Figure 4. Indicial lift under a uniform flow due to a step input with σ = 180° for various blade numbers.

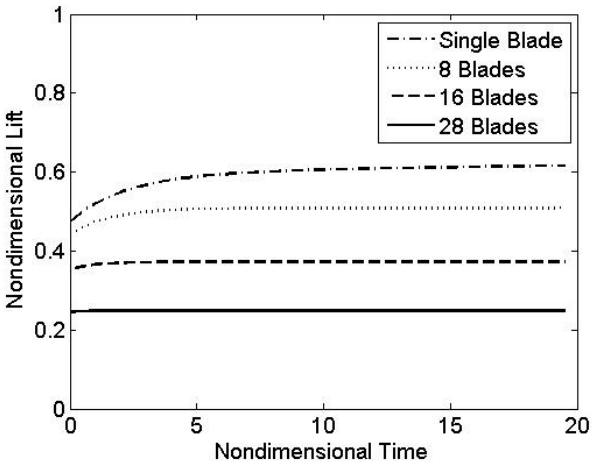

Figure 5. Indicial lift under a uniform flow due to a step input with σ = 0° for various blade numbers.

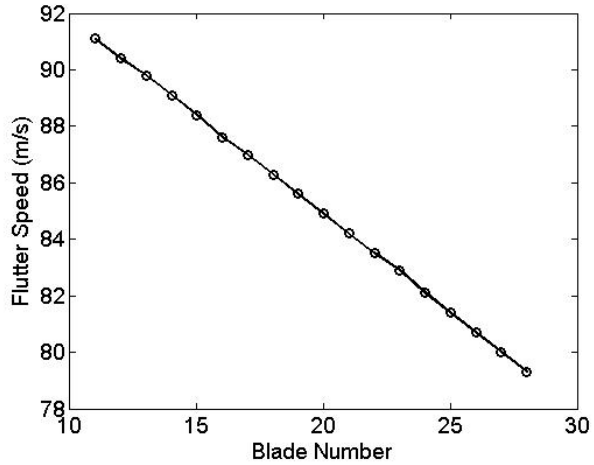

Figure 6. Flutter speed as a function of blade number.

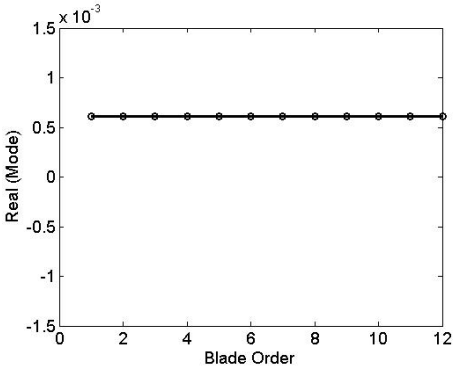

(a) Mode 0

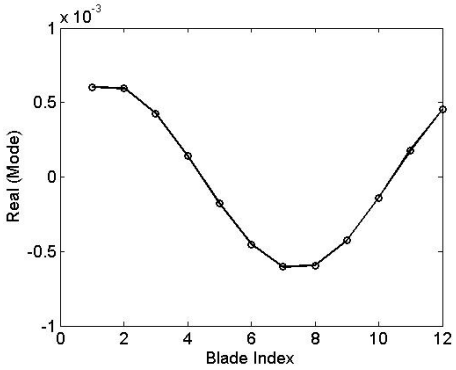

(b) Mode 1

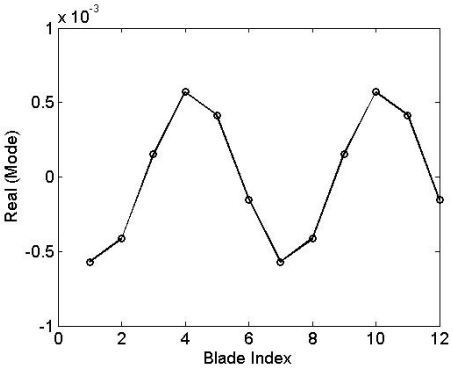

(c) Mode 2

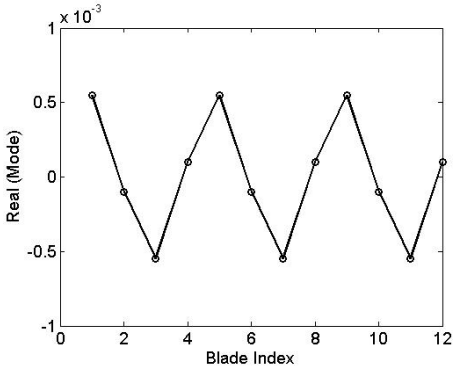

(d) Mode 3

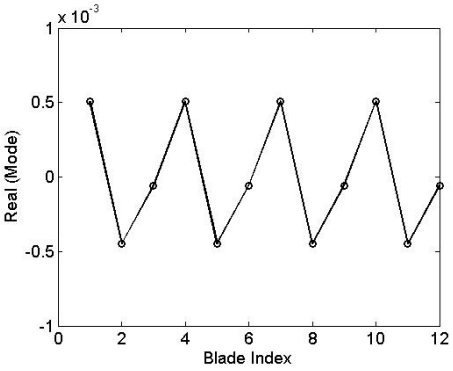

(e) Mode 4

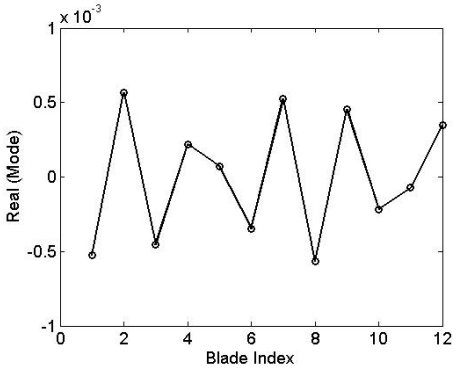

(f) Mode 5

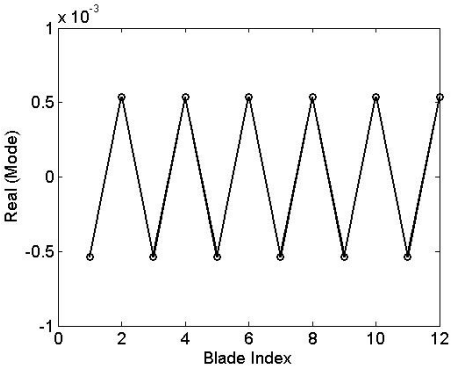

(g) Mode 6

Figure 7. Real value of eigenmodes for each blade.